Original Article

Immunohistochemical expression of osteopontin and collagens in choroid plexus of human brains

Keiji Wakamatsu,[1] Yoichi Chiba,[1] Ryuta Murakami,[1] Koichi Matsumoto,[1] Yumi Miyai,[1] Machi Kawauchi,[1] Ken Yanase,[2] Naoya Uemura[2] and Masaki Ueno[1] [ID]

Departments of [1]Pathology and Host Defense, Faculty of Medicine and [2]Anesthesiology, Faculty of Medicine, Kagawa University, Takamatsu, Japan

Evidence showing the functional significance of the choroid plexus is accumulating. Although it is clinically well-known that calcification is frequently seen in the choroid plexus of aged human brains, it is unclear why calcification occurs in the aged choroid plexus and what exert effects on the calcification has. In this study, immunohistochemical localizations of collagens and other molecules related to fibrosis or calcification were investigated on the choroid plexus of autopsied human brains. Densely fibrous or calcified materials were located in the stroma just below the epithelial cells of the choroid plexus of all human brains examined. Immunoreactivity for collagen type I was identified in the stroma just below the epithelial cells, consistent with the densely fibrous or calcified area, whereas that for collagen type III was observed in almost all stroma other than the densely fibrous or calcified areas. Linear or membranous immunoreactivity for collagen type IV was intermittently localized on the epithelium-facing side of the materials, suggesting an injured basement membrane. In addition, clear immunoreactivity for osteopontin was localized on the epithelium-facing side of the fibrous or calcified materials as well as in the cytoplasm of epithelial cells. These findings indicate that collagen type I exists in contact with osteopontin in and around the densely fibrous or calcified materials in the choroid plexus. They suggest that the densely fibrous or calcified materials are deposited in the subepithelial stroma just below an injured basement membrane of epithelial cells via the collagen type I and osteopontin.

INTRODUCTION

Evidence that the choroid plexus plays a central role not only in regulation of the microenvironment of the central nervous system by secreting most of the cerebrospinal fluid (CSF)[1,2] but also in adjustment of the circadian rhythm[3] is accumulating. Accordingly, it is reasonable to consider that damage to the choroid plexus induces brain dysfunction. Altered choroid plexus function is responsible for impaired amyloid-β clearance in a triple transgenic mouse model of Alzheimer's disease.[4] In addition, several kinds of morphological and molecular abnormalities have been reported in the choroid plexus of human brains.[5–7] As one of the morphological findings, fibrosis is known to be observed in the choroid plexus filtration membrane.[8] The number of choroid plexus psammoma bodies increases with aging.[5] Clinically, calcification of the choroid plexus is frequently noted in the aged human brain. Yalcin *et al.*[9] investigated the rate of calcification in some brain regions of 11 941 subjects by brain computed tomography (CT) and reported that 70.2% had choroid plexus calcification. The most marked age-related increase in the rate of calcification was observed in the choroid plexus among cerebral vessels and five brain regions: the choroid plexus, pineal gland, habenula, dura mater, and basal ganglia. These clinical findings suggest that the interstitial fluid flow in the stroma is stagnant, and CSF production is impaired in the choroid plexus with calcification. In fact, it was reported that CSF production is reduced in the presence of healthy aging[10] and in dementia of the Alzheimer's type.[11] In addition, direct measurement of CSF production in mice revealed that aged mice show reduced CSF production, which is even lower in aged mice overexpressing amyloid-β.[12]

However, whether morphological abnormalities in the choroid plexus of aged brains can cause dysfunction of the

choroid plexus remains to be clarified. To address this issue, in this study, we investigated morphological changes and the localizations of several kinds of molecules related to fibrosis or calcification in the choroid plexus of autopsied human brains using conventional and immunohistochemical methodologies.

MATERIALS AND METHODS

Human brain samples were obtained at autopsy from 10 patients with or without neurological disorders at Kagawa University Hospital, as previously reported.[13,14] Brief clinical information on the 10 patients is shown in Table 1. The main diagnosis of each patient was established according to clinical and autopsy findings.[13,14] This study using human brains was approved by the institutional ethics committee of the Faculty of Medicine, Kagawa University. The brains were fixed in 10% buffered formalin and processed for classical histochemical and immunohistochemical examinations. The brain samples were embedded in paraffin and sectioned at a thickness of 4 μm. At first, the sections were stained with hematoxylin and eosin (HE), Azan, and Elastica van Gieson (EVG) for evaluation of fibrous structures of the choroid plexus according to procedures reported previously.[15] In addition, modified von Kossa staining was performed using a calcium stain kit according to the attached instructions (ScyTek, Utah, USA).[15]

Next, immunohistochemical examination was performed on choroid plexus sections.[13,14] Information on the primary antibodies used in this study is summarized in Table 2.[5,13,16–24] Primary antibodies against collagen type I (col-1) (rabbit polyclonal, Cat. No. 14695-1-AP; ProteinTech Group, Chicago, IL, USA; 1:2000),[16] col-1 (mouse monoclonal, clone 3D5E8; ProteinTech; 1:1000–3000),[17] col-3 (rabbit polyclonal, Cat. No. 22734-1-AP; ProteinTech; 1:500),[18] col-4 (rabbit polyclonal, Cat. No. 55131-1-AP; ProteinTech; 1:500),[19] col-5 (mouse monoclonal, clone 2C2C2; ProteinTech; 1:500), osteopontin (rabbit polyclonal, Cat. No. 22952-1-AP;

ProteinTech; 1:100),[20] osteopontin (mouse monoclonal, clone 53; Abcam, Cambridge, UK; 1:100),[21] vimentin (mouse monoclonal, clone V9; Dako, Glostrup, Denmark; 1:50),[5,13] vimentin (rabbit monoclonal, clone SQab1721; Arigo, Hsinchu, Taiwan; 1:1000),[22] pancytokeratin (pan-CK) (mouse monoclonal, clone AE1/AE3; Dako; 1:50), α-smooth muscle actin (α-SMA) (mouse monoclonal, clone 1A4; Dako; 1:50), cluster of differentiation (CD) 34 (CD34) (mouse monoclonal, clone QBEnd10; Dako; 1:25), CD68 (mouse monoclonal, clone PG-M1; Dako; 1:50),[23] and anion exchange protein 2 (AE2) (mouse monoclonal, clone D-3; Santa Cruz Biotechnology, Dallas, TX, USA; 1:100)[24] were used in this study. Immunohistochemical expression of specific substances for epithelial and mesenchymal cells were also verified using antibodies against pan-CK and vimentin and antibodies against α-SMA, vimentin, CD34, and CD68, respectively. In addition, immunohistochemical expression of AE2, an anion exchanger of the epithelial cell, was used to confirm the functioning of epithelial cells in the choroid plexus of autopsied human brains. Before incubation with some antibodies, antigen retrieval was performed by heating sections in 10 mM sodium citrate buffer (pH 6) or 1 mM tris(hydroxymethyl)aminomethane/ethelenediamine tetraacetic acid (Tris-EDTA) buffer (pH 9) at 95°C for 20 min, as shown in Table 2. After treatment with hydrogen peroxide and blocking with 2% bovine serum albumin in phosphate-buffered saline (PBS) for 30 min, the sections were incubated overnight at 4°C with the primary antibodies. After washing the sections with PBS, staining was achieved with a Simple Stain kit (Nichirei, Tokyo, Japan) and developed with 3,3′-diaminobenzidine tetrahydrochloride (DAB) and hydrogen peroxide (Nichirei) at room temperature (RT) for 5–7 min. The sections were counterstained with hematoxylin.

For double-labeled immunofluorescence staining, the sections were incubated overnight at 4°C with the mouse antibody to col-1 or osteopontin, and the rabbit antibody to osteopontin, col-1, col-3, or col-4, followed by

Table 1 Summary of clinicopathological profiles of cases examine

Number	Age/Sex	Main diagnosis	Azan	Col-1	Col-3	Osp
1	57/F	Psychiatric disorder, liver abscess, Sepsis	42.8% (2.2%)	2+	2+	1+
2	68/F	Thalamic hemorrhage	50.7% (1.7%)	2+	2+	1+
3	72/F	Pneumonia	43.5% (2.2%)	2+	2+	2+
4	42/M	Pulmonary hypertension, heart failure	66.4% (0.2%)	2+	1+	1+
5	64/M	Multiple system atrophy, pneumonia	59.6% (2.3%)	2+	1+	2+
6	70/M	Myocardial infarction	72.3% (3.0%)	2+	2+	2+
7	74/M	Lung cancer	54.7% (2.0%)	2+	2+	1+
8	75/M	Gastric cancer	54.6% (0.8%)	2+	2+	2+
9	75/M	Multiple system atrophy, pneumonia	46.5% (3.3%)	2+	2+	2+
10	84/M	Myocardial infarction, cerebral infarction	24.5% (0.5%)	2+	1+	1+

The area in parentheses is the ratio of the deeply stained area to the total stromal area. F, female; M, male.

Table 2 Summary of antibodies used in this study

Antigen	Cat. No./clone	Host species and dilution	References
Collagen type I (Col-1)	14 695-1-AP	Rabbit, 1:2000[‡]	16
Collagen type I (Col-1)	66 761-1-lg (3D5E8)	Mouse, 1:1000-3000[‡]	17
Collagen type III (Col-3)	22 734-1-AP	Rabbit, 1:500[‡]	18
Collagen type IV (Col-4)	55 131-1-AP	Rabbit, 1:500[‡]	19
Collagen type V (Col-5)	67 604-1-lg (2C2C2)	Mouse, 1:500[‡]	
Osteopontin	22 952-1-AP	Rabbit, 1:100	20
Osteopontin	ab69498 (53)	Mouse, 1:100[‡]	21
Vimentin	M0725 (V9)	Mouse, 1:50[†]	5,13
Vimentin	ARG66199 (SQab1721)	Rabbit, 1:1000[‡]	22
Pancytokeratin (Pan-CK)	M3515 (AE1/AE3)	Mouse, 1:50[‡]	
α-SMA	M0851 (1A4)	Mouse, 1:50[‡]	
CD34	M7165 (QBEnd10)	Mouse, 1:25[‡]	
CD68	M0876 (PG-M1)	Mouse, 1:50[‡]	23
AE2	sc-376 632 (D-3)	Mouse, 1:100[†]	24

[†]Antigen retrieval with citrate buffer (pH 6) is needed prior to the application of the primary antibody. [‡]Antigen retrieval with Tris-EDTA buffer (pH 9) is needed prior to the application of the primary antibody.

incubation for 60 min at RT in Alexa Fluor-conjugated secondary antibodies (Molecular Probes, Eugene, OR, USA; 1:200). Before incubation with the primary antibodies, antigen retrieval was performed by heating sections in 10 mM sodium citrate buffer (pH 6) or 1 mM Tris-EDTA (pH 9) for 20 min at 95°C. The sections were then incubated for 60 min at RT in Monomeric Cyanine Nucleic Acid Stain (TOPRO-3; Molecular Probes, Eugene, OR, USA), which was diluted to 2.5 μM in PBS. The fluorescent signals were viewed under a confocal microscope (LSM700; Carl Zeiss, Oberkochen, Germany). As a control experiment, we performed an identical immunohistochemical procedure with omission of the primary antibodies.

Morphometrical analyses of stromal fibrosis of the choroid plexus were performed. The area ratio of the region positively stained with Azan staining to the total stromal area was calculated using image processing software (ImageJ; US National Institutes of Health). Immunoreactivities for col-1 (14 695-1-AP) and osteopontin (22 952-1-AP) were analyzed as follows; clear or faint positive immunostaining in the fibrotic foci was evaluated as 2+ or 1+, respectively. Immunoreactivity for col-3 was analyzed as follows; diffusely or focally clear positive staining in almost all stromal areas except for the fibrotic foci was evaluated as 2+ or 1+, respectively.

RESULTS

Ten images on HE staining (Fig. 1A–J) correspond in order to the 10 patients introduced in Table 1. HE staining revealed that densely fibrous or calcified materials were localized in the stroma just below the epithelial cells of the choroid plexus of all human brains examined. Azan staining revealed that fine fibrous tissues were widespread in the stroma of the choroid plexus (Fig. 1K). EVG staining revealed that densely fibrous materials were present in the stroma of the choroid plexus, and, moreover, that densely fibrous or calcified materials contained no elastic fibers (Fig. 1L). Modified von Kossa staining revealed that some densely fibrous materials contained calcium crystals (Fig. 1M). Enlarged images on HE (Fig. 1C), Azan (Fig. 1K), EVG (Fig. 1L), and modified von Kossa (Fig. 1M) staining emphasized the calcified materials and also revealed that epithelial cells just above the calcified materials were thin or absent (Fig. 1C, K). In addition, spindle-shaped mesenchymal cells were occasionally localized around the calcified materials (Fig. 1B, J, L).

Immunohistochemical examination using antibodies to fibril-forming collagens (col-1, col-3, and col-5), basement membrane-forming collagen col-4, osteopontin, vimentin, α-SMA, pan-CK, CD34, CD68, and AE2 were performed (Fig. 2A–O). Immunoreactivity for col-1 was observed in the densely fibrous or calcified materials (Fig. 2A), whereas that for col-3 was observed in almost all stroma other than the densely fibrous or calcified areas (Fig. 2B). Immunoreactivity for col-5 was not clear in the calcified areas of the choroid plexus (Fig. 2C). Immunoreactivity for col-4 in the epithelial basement membrane was intermittently observed on the epithelium-facing side of the calcified materials (Fig. 2D). Immunoreactivities with the rabbit (Fig. 2E) and mouse (Fig. 2F) antibodies to osteoponti were observed on the epithelium-facing side of the calcified materials just below thin epithelial cells as well as in the cytoplasm of the epithelial cells. Immunoreactivities with the mouse (Fig. 2G) and rabbit (Fig. 2H) antibodies to vimentin were occasionally observed in the cytoplasm of spindle-shaped mesenchymal cells around the densely fibrous or calcified materials as well as in the cytoplasm of epithelial cells. Immunoreactivity for α-SMA was observed
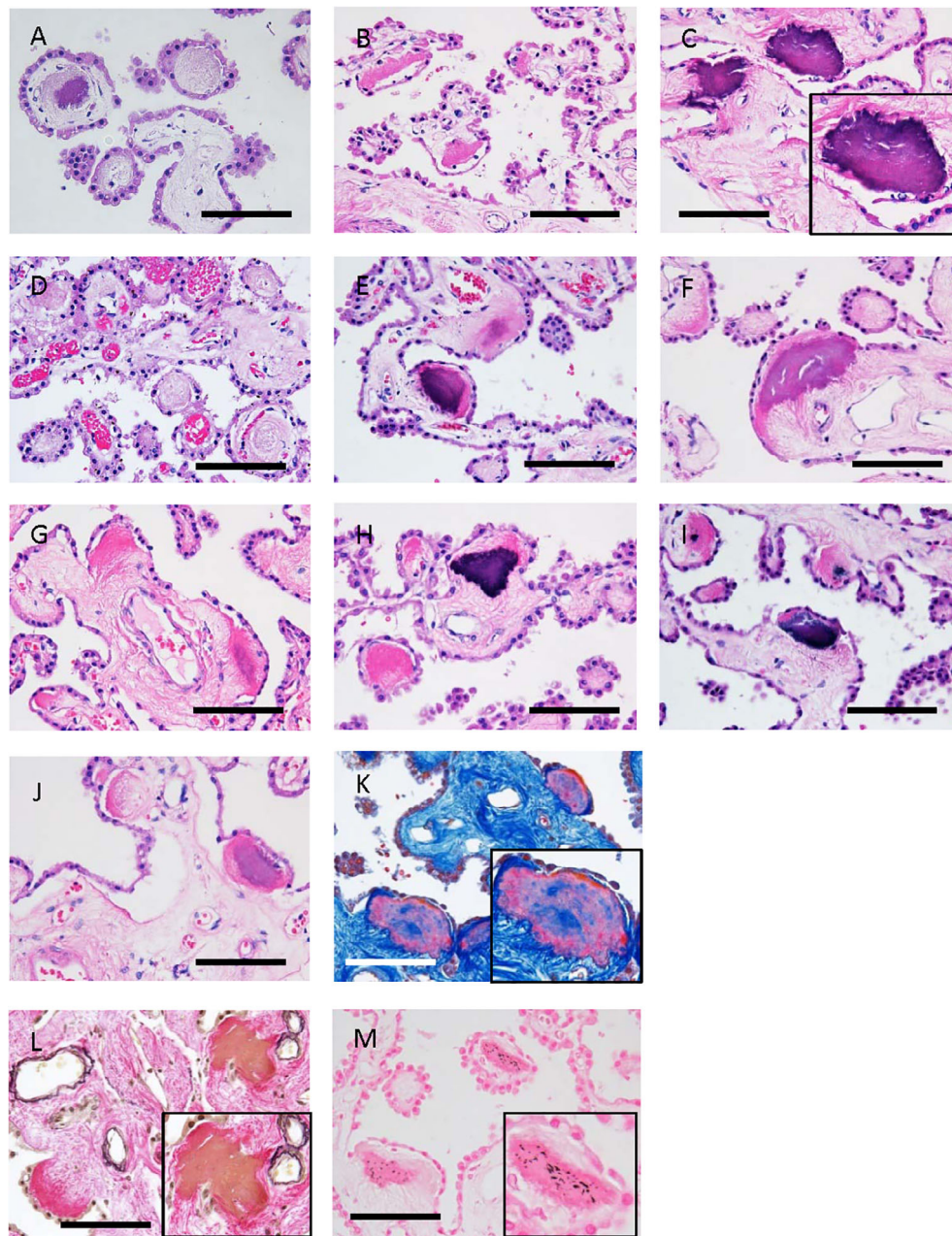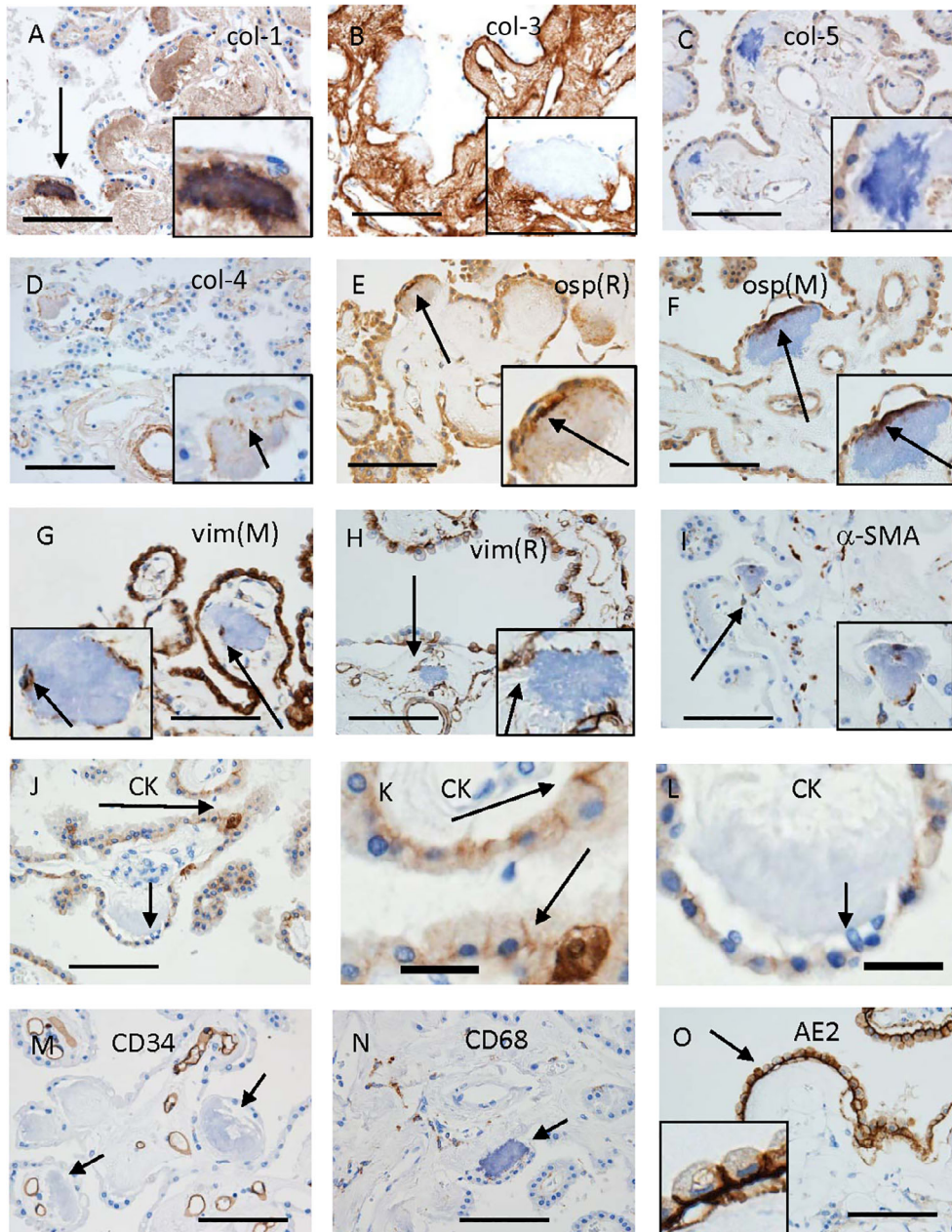
Fig 1 Microphotographs of the choroid plexus taken from cases 1 (A), 2 (B), 3 (C), 4 (D), 5 (E), 6 (F, K, L), 7 (G), 8 (H, M), 9 (I), and 10 (J). (A-M) Densely fibrous or calcified areas are shown in each inset. HE (A-J), Azan (K), EVG (L), modified von Kossa (M). Scale bars: 100 μm (A–M).

in a few spindle-shaped mesenchymal cells around the calcified materials (Fig. 2I). In addition, immunoreactivity for pan-CK was generally observed in the cytoplasmic membrane of epithelial cells (arrows in Fig. 2J, K), whereas it was very weak or absent in epithelial cells just above the calcified materials (short arrow in Fig. 2J, L). In addition, CD34-immunoreactive cells, including endothelial cells (Fig. 2M) and CD68-immunoreactive macrophages (Fig. 2N) were not observed in the calcified materials. Immunoreactivity for AE2 was clearly observed in the basolateral plasma membrane of epithelial cells (Fig. 2O). All images on Azan and EVG staining as well as

immunoreactivities for col-1, col-3, and osteopontin in the 10 autopsied brains are shown in Figure S1. The results of morphometrical analyses for fibrosis and immunohistochemistry are shown in Table 1.
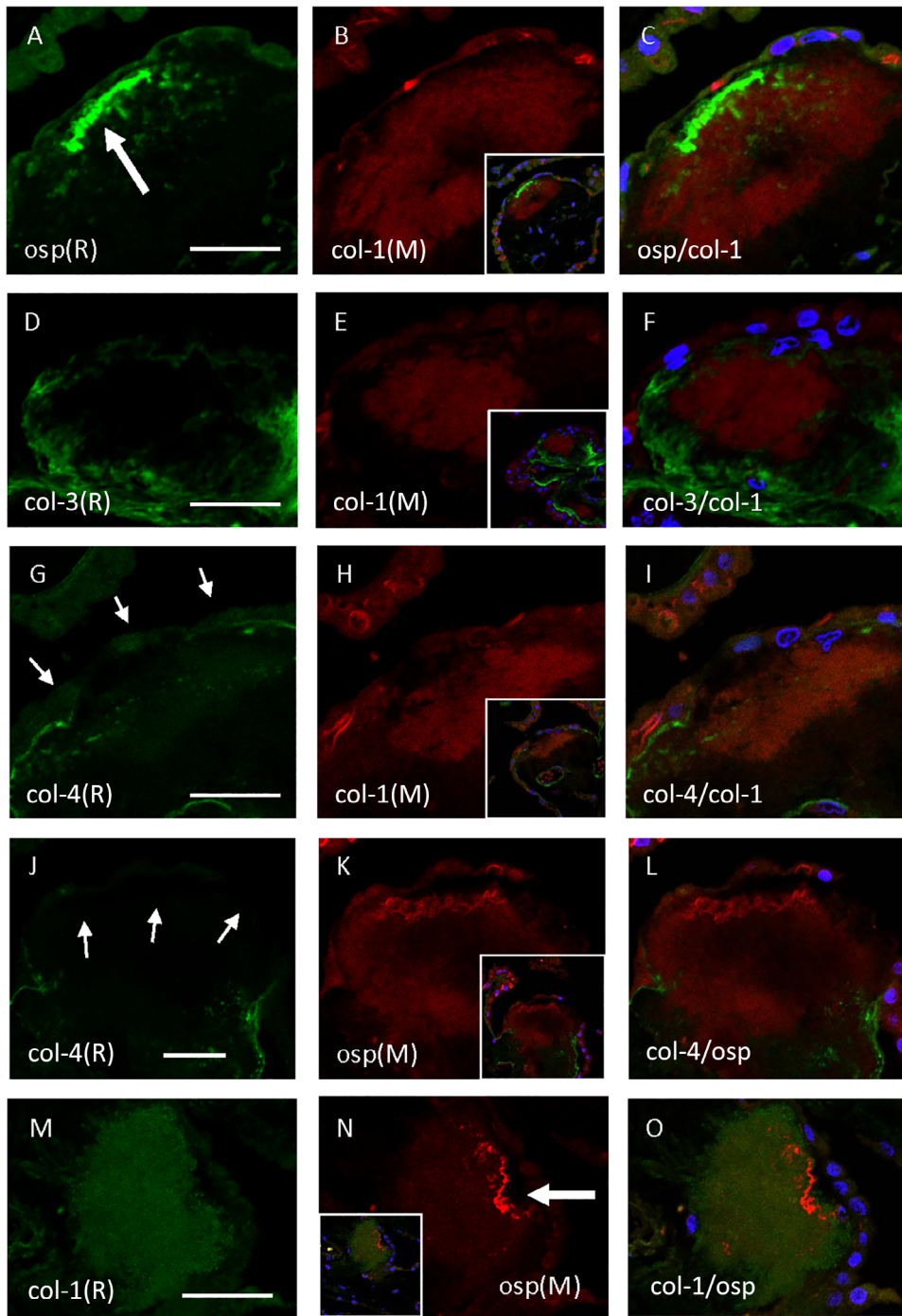
Double-labeled immunofluorescence staining revealed that immunoreactivity for osteopontin existed in concert with that for col-1 in and around the epithelium-facing side of the calcified materials (Fig. 3A–C), whereas immunoreactivity for col-3 was not colocalized with that for col-1 in the stroma (Fig. 3D–F). Immunoreactivity for col-4 in the basement membrane partially (short arrows in Fig. 3G, J)

Fig 2 Immunohistochemical findings of the choroid plexus from cases 2 (D), 3 (A, C), 6 (B, E, F), 8 (H, I), and 10 (G, J-O). Insets of (A–I, O) show enlarged images of their microphotographs. Immunoreactivity shown by long arrows in (A, E, F) is observed in calcified materials. Short arrows in (D) show intermittent staining. Long arrows in (G–I) indicate immunoreaction in spindle-shaped mesenchymal cells attached to or located around the calcified materials. (K) and (L) are enlarged images indicated by long and short arrows in (J), respectively. Long arrows in (K) indicates clear immunoreactivity in the cytoplasmic membrane of other epithelial cells, whereas a short arrow in (L) indicates no or weak immunoreactivity for pan-CK in epithelial cells just above the calcified materials. Short arrows in (M, N) indicate no immunoreactivities for CD34 and CD68 in calcified materials, respectively. Immunohistochemistry for col-1 (A), col-3 (B), col-5 (C), col-4 (D), and osteopontin (osp) with rabbit (E) and mouse (F) antibodies, for vimentin (vim) with mouse (G) and rabbit (H) antibodies, antibodies, and for α-SMA (I), pan-CK (CK) (J–L), CD34 (M), CD68 (N), and AE2 (O). Scale bars: 100 μm (A–J, M–O), 20 μm (K, L).

disappeared in subepithelial areas just above the materials immunoreactive for col-1 (Fig. 3G–I) or osteopontin (Fig. 3J–L). Immunoreactivity with the mouse antibody to osteopontin existed in concert with that with the rabbit antibody to col-1 on and around the epithelium-facing side of the calcified materials (Fig. 3M–O).

Fig 3 Representative confocal microscopic images on double-labeled immunofluorescence staining. Left column images indicate panels (green), middle column images indicate panels (red), and right column panels indicate merged images of the left and middle panels of the same line with nuclear staining with TO-PRO-3 (blue). An inset of each image in (B, E, H, K, N) shows an original merged image. Thick arrows in images (A, N) show immunoreactivity for osteopontin in contact with materials immunoreactive for col-1. Three short arrows in (G, J) partially show the absence of col-4 in the basement membrane of epithelial cells. Abbreviations: col-1, collagen type I; col-3, collagen type III; col-4, collagen type IV; osp, osteopontin; (M), mouse antibody; (R), rabbit antibody. Scale bars: 50 μm.

DISCUSSION

In this study, densely fibrous or calcified materials were localized in the stroma just below epithelial cells of the choroid plexus of 10 human brains. Accordingly, immunoreactivities for fibril-forming collagens (col-1, col-3, and col-4) were first.[25] The densely fibrous or calcified materials were immunoreactive for col-1. In contrast, the stroma other than the calcified materials was filled with finely fibrous tissues immunoreactive for col-3. Clore *et al.*[26] reported that col-3 appears first as an early collagen in granulation tissue, which in turn is gradually replaced by col-1 in a healing wound. As immunoreactivity for col-4 in the epithelial basement membrane was intermittently observed on the epithelium-facing side of the calcified materials immunoreactive for col-1, the basement membrane was considered to be partially injured there. Therefore, similar tissue repair may also occur in the choroid

plexus of aged brains. Elastic fibers were undetectable in the calcified materials, indicating the lack of a link between the materials and vessel wall. Some materials contained calcium crystals. These findings indicate that calcification occurred in the stroma just below the injured basement membrane of epithelial cells but not in perivascular areas. From the results shown in Table 1, multiple factors, including aging, vascular diseases, infectious diseases, and neurodegenerative diseases, may affect the expression of osteopontin and collagens in the choroid plexus. Further large-scale analytical studies are necessary to identify the factors.

Osteopontin is known to promote col-1 synthesis in hepatic stellate cells.[27] Osteopontin overproduction is associated with the progression of glomerular fibrosis.[28] Regarding the expression of substances related to calcification, osteopontin expression was reported to be associated with the appearance of psammoma bodies in thyroid carcinoma cells,[29] suggesting that osteopontin is the main contributor to matrix calcification. In addition, osteopontin was reported to be responsible for the process of biomineralization, as observed in psammoma bodies in papillary thyroid carcinoma[30] and ovarian cancer.[31] Immunohistochemical expression of osteopontin is localized in epithelial cells of the normal human choroid plexus.[32] In this study, we also observed immunoreactivity for osteopontin in the cytoplasm of epithelial cells of the choroid plexus. In addition, clear immunoreactivity for osteopontin was observed in the stroma just below the injured basement membrane of epithelial cells and on and around the epithelium-facing side of the calcified materials immunoreactive for col-1 (Fig. 3A–C). Thus, it is likely that expression of osteopontin in the stroma just below epithelial cells induces overproduction of col-1, considered to be followed by mineralization.

In addition, immunohistochemical examination of epithelial and mesenchymal cells in the choroid plexus was performed to determine the relationship between densely fibrous materials and epithelial or mesenchymal cells. Normal choroid plexus epithelium and choroid plexus papillomas were reported to be immunohistochemically positive for prealbumin, S-100 protein, cytokeratin, and vimentin.[33] Also in this study, immunohistochemical expression of cytokeratin and vimentin was observed in epithelial cells of the choroid plexus. Moreover, AE2, an anion exchanger of the epithelial cells,[34] was confirmed to be immunohistochemically expressed in the basolateral plasma membrane of epithelial cells in the choroid plexus of autopsied human brains. In this study, immunoreactivities for α-SMA and vimentin in spindle-shaped mesenchymal cells were observed around the calcified materials. It is known that fibroblasts proliferate and convert to myofibroblasts in the later phase of wound healing.[35]

Accordingly, these mesenchymal cells that are immunoreactive for vimentin and α-SMA may be involved in the repair of tissues of the choroid plexus.

This study showed that the parenchyma of the choroid plexus of aged brains exhibited extensive fibrosis, partially with calcification. In addition, immunoreactivities for col-1 and osteopontin coexisted in contact with each other in and around the calcified materials in the choroid plexus. These abnormal findings may be related to choroid plexus dysfunction, presumably due to flow obstruction of interstitial fluids, including nutrients. Myung *et al.*[3] reported that the choroid plexus is an important circadian clock component, suggesting a great role of the choroid plexus in adjusting circadian rhythm. In addition, it has become well-known that numerous transporters are localized in epithelial cells of the choroid plexus,[36–38] indicating more transportation functions of choroid plexus epithelial cells than previously considered those. From these findings, it is likely that choroid plexus dysfunction has significant effects on various brain functions, including cognitive function. Further studies, including large-scale analytical, experimental animal, and *in vitro* studies, are required to clarify the roles of the choroid plexus in various brain dysfunctions.

ACKNOWLEDGMENTS

DISCLOSURE

REFERENCES

1. Lun MP, Johnson MB, Broadbelt KG *et al*. Spatially heterogeneous choroid plexus transcriptomes encode positional identity and contribute to regional CSF production. *J Neurosci* 2015; **35**: 4903–4916.

2. Bryniarski MA, Ren T, Rizvi AR, Snyder AM, Morris ME. Targeting the choroid plexuses for protein drug delivery. *Pharmaceutics* 2020; **12**: 963.

3. Myung J, Schmal C, Hong S *et al*. The choroid plexus is an important circadian clock component. *Nat Commun* 2018; **9**: 1062.

4. González-Marrero I, Giménez-Llort L, Johanson CE *et al*. Choroid plexus dysfunction impairs beta-amyloid clearance in a triple transgenic mouse model of Alzheimer's disease. *Front Cell Neurosci* 2015; **9**: 17.

5. Jovanović I, Ugrenović S, Antić S, Stefanović N, Mihailović D. Morphometric and some immunohisto-chemical characteristics of human choroids plexus stroma and psammoma bodies. *Microsc Res Tech* 2007; **70**: 617–627.

6. Jovanović I, Ugrenović S, Vasović L, Petrović D, Cekić S. Psammoma bodies – Friends or foes of the aging choroid plexus. *Med Hypotheses* 2010; **74**: 1017–1020.

7. Pearson A, Ajoy R, Crynen G *et al.* Molecular abnor-malities in autopsied brain tissue from the inferior horn of the lateral ventricles of nonagenarians and Alzheimer disease patients. *BMC Neurol* 2020; **20**: 317.

8. Prineas JW, Parratt JDE, Kirwan PD. Fibrosis of the choroid plexus filtration membrane. *J Neuropathol Exp Neurol* 2016; **75**: 855–867.

9. Yalcin A, Ceylan M, Bayraktutan OF, Sonkaya AR, Yuce I. Age and gender related prevalence of intra-cranial calcifications in CT imaging; data from 12,000 healthy subjects. *J Chem Neuroanat* 2016; **78**: 20–24.

10. May C, Kaye JA, Atack JR, Schapiro MB, Friedland RP, Rapoport SI. Cerebrospinal fluid pro-duction is reduced in healthy aging. *Neurology* 1990; **40**: 500–503.

11. Silverberg GD, Heit G, Huhn S *et al.* The cerebrospi-nal fluid production rate is reduced in dementia of the Alzheimer's type. *Neurology* 2001; **57**: 1763–1766.

12. Liu G, Mestre H, Sweeney AM *et al.* Direct mesurement of cerebrospinal fluid production in mice. *Cell Rep* 2020; **33**: 108524.

13. Matsumoto K, Chiba Y, Fujihara R, Kubo H, Sakamoto H, Ueno M. Immunohistochemical analysis of transporters related to clearance of amyloid-β pep-tides through blood-cerebrospinal fluid barrier in human brain. *Histochem Cell Biol* 2015; **144**: 597–611.

14. Chiba Y, Sugiyama Y, Nishi N, Nonaka W, Murakami R, Ueno M. Sodium/glucose cotransporter 2 is expressed in choroid plexus epithelial cells and ependymal cells in human and mouse brain. *Neuropa-thology* 2020; **40**: 482–491.

15. Fujihara R, Chiba Y, Nakagawa T *et al.* His-tomorphometry of ectopic mineralization using undecalcified frozen bone sections. *Microsc Res Tech* 2018; **81**: 1318–1324.

16. Rong L, Huang W, Tian S, Chi X, Zhao P, Liu F. COL1A2 is a novel biomarker to improve clinical pre-diction in human gastric cancer: Integrating bioinfor-matics and meta-analysis. *Pathol Oncol Res* 2018; **24**: 129–134.

17. Xu X, Yu H, Sun L *et al.* Adipose-derived mesenchymal stem cells ameliorate dibutyltin dichloride-induced chronic pancreatitis by inhibiting the PI3K/AKT/mTOR signaling pathway. *Mol Med Rep* 2020; **21**: 1833–1840.

18. Kumagai M, Guo X, Wang K-Y *et al.* Depletion of WNT10A prevents tumor growth by suppressing microvessels and collagen expression. *Int J Med Sci* 2019; **16**: 416–423.

19. Shang J, Wang L, Zhang Y *et al.* Chemerin/ChemR23 axis promotes inflammation of glomerular endothelial cells in diabetic nephropathy. *J Cell Mol Med* 2019; **23**: 3417–3428.

20. Si J, Dai J, Zhang J *et al.* Comparative investigation of human amniotic epithelial cells and mesenchymal stem cells for application in bone tissue engineering. *Stem Cells Int* 2015; **2015**: 565732.

21. Byeon H, Lee SD, Hong E-K *et al.* Long term prog-nostic impact of osteopontin and Dickkopf-related protein 1 in patients with hepatocellular carcinoma after hepatectomy. *Pathol Res Pract* 2018; **214**: 814–820.

22. Li S, Cong X, Gao H *et al.* Tumor-associated neutro-phils induce EMT by IL-17a to promote migration and invasion in gastric cancer cells. *J Exp Clin Cancer Res* 2019; **38**: 6.

23. Mashima M, Chiba Y, Murakami R *et al.* Glucose transporter 8 immunoreactivity in astrocytic and microglial cells in subependymal areas of human brains. *Neurosci Lett* 2017; **636**: 90–94.

24. Itoh R, Hatano N, Murakami M *et al.* Both IRBIT and long-IRBIT bind to and coordinately regulate Cl^-/HCO_3^- exchanger AE2 activity through modulat-ing the lysosomal degradation of AE2. *Sci Rep* 2021; **11**: 5990.

25. Gelse K, Poschl E, Aigner T. Collagens – Structure, function, and biosynthesis. *Adv Drug Deliv Rev* 2003; **55**: 1531–1546.

26. Clore JN, Cohen IK, Diegelmann RF. Quantitation of collagen types I and III during wound healing in rat skin. *Proc Soc Exp Biol Med* 1979; **161**: 337–340.

27. Chen Y, Ou Y, Dong J *et al.* Osteopontin promotes collagen I synthesis in hepatic stellate cells by miRNA-129-5p inhibition. *Exp Cell Res* 2018; **362**: 343–348.

28. Merszei J, Wu J, Torres L *et al.* Osteopontin over-production is associated with progression of glomeru-lar fibrosis in a rat model of anti-glomerular basement membrane glomerulonephritis. *Am J Nephrol* 2010; **32**: 262–271.

29. Ferreira LB, Lima RT, Bastos ACSDF *et al.* OPNa overexpression is associated with matrix calcification in thyroid cancer cell lines. *Int J Mol Sci* 2018; **19**: 2990.

30. Tunio GM, Hirota S, Nomura S, Kitamura Y. Possible relation of osteopontin to development of psammoma bodies in human papillary thyroid cancer. *Arch Pathol Lab Med* 1998; **122**: 1087–1090.

31. Maki M, Hirota S, Kaneko Y, Morohoshi T. Expression of osteopontin messenger RNA by macrophages in ovarian serous papillary cystadenocarcinoma: A possible association with calcification of psammoma bodies. *Pathol Int* 2000; **50**: 531–535.

32. Kunii Y, Niwa S, Hagiwara Y, Maeda M, Seitoh T, Suzuki T. The immunohistochemical expression profile of osteopontin in normal human tissues using two site-specific antibodies reveals a wide distribution of positive cells and extensive expression in the central and peripheral nervous systems. *Med Mol Morphol* 2009; **42**: 155–161.

33. Lach B, Scheithauer BW, Gregor A, Wick MR. Colloid cyst of the third ventricle. A comparative immunohistochemical study of neuraxis cysts and choroid plexus epithelium. *J Neurosurg* 1993; **78**: 101–111.

34. Lindsey AE, Schneider K, Simmons DM, Baron R, Lee BS, Kopito RR. Functional expression and subcellular localization of an anion exchanger cloned from choroid plexus. *Proc Natl Acad Sci U S A* 1990; **87**: 5278–5282.

35. Guillamat-Prats R. The role of MSC in wound healing, scarring and regeneration. *Cell* 2021; **10**: 1729.

36. Saunders NR, Dziegielewska KM, Møllgård K *et al*. Influx mechanism in the embryonic and adult rat choroid plexus: A transcriptome study. *Front Neurosci* 2015; **9**: 123.

37. Uchida Y, Zhang Z, Tachikawa M, Terasaki T. Quantitative targeted absolute proteomics of rat blood-cerebrospinal fluid barrier transporters: Comparison with a human specimen. *J Neurochem* 2015; **134**: 1104–1115.

38. Chiba Y, Murakami R, Matsumoto K *et al*. Glucose, fructose, and urate transporters in the choroid plexus epithelium. *Int J Mol Sci* 2020; **21**: 7230.

SUPPORTING INFORMATION

Additional supporting information may be found in the online version of this article at the publisher's website:

Figure S1. Microphotographs of Azan and EVG staining and immunostaining of col1, col3, and osteopontin in the choroid plexus of the 10 human brains (A–J). Branch numbers 1, 2, 3, 4, and 5 indicate Azan and EVG staining and immunostaining of col1, col3, and osteopontin, respectively. Arrows in A-5 to J-5 indicate fibrotic foci with immunohistochemical expression of osteopontin. Images in A–J are taken from sections of (A: No. 1), (B: No. 2), (C: No. 3), (D: No. 4), (E: No. 5), (F: No. 6), (G: No. 7), (H: No. 8), (I: No. 9), and (J: No. 10), respectively. Scale bars: 100 μm.